Micromechanics of reinforcement of a graphene-based thermoplastic elastomer nanocomposite

DOI:
10.1016/j.compositesa.2018.04.014

Document Version
Accepted author manuscript

Micromechanics of reinforcement of a graphene-based thermoplastic elastomer nanocomposite

Mufeng Liu, Dimitrios G. Papageorgiou*, Suhao Li, Kailing Lin, Ian A. Kinloch,

Robert J. Young*

School of Materials and National Graphene Institute, University of Manchester, Oxford Road, M13 9PL, Manchester, United Kingdom

Corresponding authors: dimitrios.papageorgiou@manchester.ac.uk,

robert.young@manchester.ac.uk

Abstract: In this work, a series of graphene-reinforced thermoplastic elastomers were prepared, with the introduction of graphene nanoplatelets (GNPs) of different particle diameter. Their microstructures were characterised by SEM and quantified by polarised Raman spectroscopy. The GNPs were well-dispersed and their orientation across the cross-section of the injection moulded samples was consistent with the shear rate profile of fountain flow mechanism. The mechanical properties of the nanocomposites were evaluated by tensile testing and it was found that the GNPs contributed to significant improvements in both the stiffness and strength. A micromechanical model based on the combination of shear-lag theory and the rule-of-mixtures was introduced to analyse the stiffening mechanisms. The effective aspect ratio of GNPs was in the order of 100 and decreased with increasing filler loading due to agglomeration. Finally, the stress transfer efficiency from the matrix to GNPs was evaluated by observing the Raman band shifts under tension.

Keywords: A. nanocomposites; A. graphene; B. stress transfer; C. micromechanics

1. Introduction

Thermoplastic elastomers (TPEs) based on thermoplastic vulcanizate blends are considered an interesting class of materials since they combine the melt processability of thermoplastics with the properties of conventional thermoset rubbers [1]. The TPEs usually have excellent weatherability, ozone resistance, chemical resistance to oils and abrasion resistance; however, their applications are limited by their relatively poor mechanical properties [2]. In this context, inorganic fillers have been incorporated within the TPEs and enhancements in their mechanical performances have been reported in the literature [3-7]. More recently, since the isolation of monolayer graphene [8] and the discovery of its unique properties, graphene and graphene-related nanomaterials have been employed extensively as reinforcement in elastomers [9].

It has been reported previously that although the intrinsic Young's modulus of monolayer graphene has been found to be very high (~1 TPa) [10, 11], it cannot be fully utilized in bulk nanocomposites, especially in soft materials such as elastomers due to inefficient stress transfer from the low modulus matrix to the high modulus filler by shear at the filler/matrix interface [9, 12-17]. In addition, we showed recently that classical micromechanics can be applied for the study of the mechanisms of stress transfer in polymeric matrices with varying stiffness and a theory was developed, which can predict the modulus of bulk nanocomposites based on the characteristics of the nanoplatelets [15, 17]. The reinforcing mechanism of elastomers reinforced by graphene is different from that of stiff polymers: the normalized modulus of an elastomer/graphene nanocomposite is dependent upon the graphene orientation, the aspect ratio and volume fraction of the filler, while it is independent of the filler modulus [17]. This result suggests that the filler geometry and the processing methods (which in turn affect the nanoscale filler distribution [9, 18]) will eventually determine the mechanical properties of the elastomeric nanocomposites.

In the present work, we have undertaken a comprehensive study of the mechanisms of reinforcement of a TPE by GNPs. The composite samples based on a thermoplastic elastomer

(Alcryn®) and GNPs with three different flake sizes were prepared by melt mixing. The microstructure of the injection moulded specimen was studied by quantifying the orientation factor of the fillers with polarised Raman spectroscopy. The mechanical properties of the nanocomposites with different filler loadings were evaluated by tensile testing followed by stress transfer measurements by observing the 2D Raman band shifts of the fillers during *in situ* deformation. Moreover, we applied our recently developed theory [17] to the experimental results from tensile testing and correlated the fittings with important geometrical characteristics of the filler, such as the effective aspect ratio. Through the experimental and theoretical analysis, we can conclude that the enhancement of thermoplastic elastomers with graphene nanoplatelets is effective, and gives considerable potential to develop high-performance engineering plastics, with tuned, application-specific properties.

2. Experimental Methods

2.1 Materials and preparation

Graphene nanoplatelets (GNPs) with nominal lateral diameters of 5, 10, 25 μm (dimensions claimed by the supplier) and average thicknesses in the range of 6-8 nanometres were purchased from XG Sciences, Inc. Lansing, Michigan, USA and used as received. Three grades of xGnP® M5, M15 and M25 were used. The thermoplastic elastomer, Alcryn® 2265 UT (Unfilled Translucent), which is based on a partially crosslinked chlorinated olefin interpolymer alloy, was purchased from A. Schulman, Inc.

The melt mixing of the composites was undertaken in a Thermo Fisher HAAKE Rheomix internal mixer. The mixing took place at 165 ^{o}C and 50 rpm for 5 minutes. The GNP fractions in the nanocomposites were 1 %, 5 %, 10 %, and 20 % by weight. The Alcryn nanocomposites in this study are coded based on the type of the matrix, the diameter and weight content of the fillers. For example, the sample code 2265-M15-GNP10, means that the matrix is the Alcryn 2265, the

diameter of the GNPs is 15 μm and the weight percentage of the filler is 10 wt%.

The dumbbell-shaped tensile specimens were prepared by injection moulding in a HAAKE Minijet Piston Injection Moulding System. The temperatures of the barrel and the mould were set as 185 ^{o}C and 30 ^{o}C. The injection pressures were 500 bar, 550 bar, 600 bar, 700 bar and 800 bar for the neat polymer and the nanocomposites filled with 1 wt%, 5 wt%, 10 wt% and 20 wt% of GNPs, respectively. The injection pressure was held for 10 seconds followed by post-injection pressure of 200 bar, held for 5 seconds, for all specimens.

2.2 Characterization of the nanocomposites

The actual loadings of GNPs in the nanocomposites were obtained by thermogravimetric analysis (TGA) using a TA Q500 TGA instrument. The samples were heated from room temperature up to 600 ^{o}C under a 50 mL/min flow of N_2 at 10^{o}C/min. Three samples were tested for each material in order to ensure reproducibility of the results.

The morphologies of the fillers, neat polymer and the microstructure of the nanocomposites were examined using scanning electron microscopy (SEM). The samples (GNP powders and cryo-fractured dumbbells) were placed on conductive carbon tapes, which were stuck on aluminium stubs. Subsequently, the coating process was carried out using Au-Pd alloy in order to provide satisfactory conductivity to the samples. The images were acquired using a high-resolution XL30 Field Emission Gun Scanning Electron Microscope (FEGSEM) at 6 kV.

The XRD diffractograms were obtained from a PANalytical X'Pert3 diffractometer with Cu Kα radiation. The 2-theta angle range was selected from 5° to 90° with a step size of 0.03^{o} and a step time of 180 s operated at 40 kV and 40 mA.

Stress–strain curves were obtained using dumbbell-shaped specimens in an Instron 4301 machine, under a tensile rate of 50 mm·min^{-1} with a load cell of 5 kN.

Raman spectra were obtained using a Renishaw InVia Raman spectrometer with a laser wavelength of 633 nm and an objective of ×50, which produces a spot size of 1-2 μm. The Raman 2D band shift of the injection moulded samples (gauge length ~ 55 mm) was studied following the application of strain on the nanocomposites with the highest loading of GNPs (20 wt%). The tests were carried out using a mini-tensile rig. The strain was determined by measuring the extension of the two grips with a digital caliper. The Raman laser spot was in the order of 1-2 μm and it was focused on the same point of a single flake on each sample surface. The results were based on 5 composite samples for each type of GNPs, at the highest loading. All the spectra were fitted with a single Lorentzian curve.

The spatial orientation of the GNPs in the composites was determined using the method reported in previous studies from our group [13, 14, 19]. The equipment employed was a 514 nm Raman spectrometer by Renishaw with 'VV' (vertical-vertical) polarisation, in which the incident and scattered radiation were polarised in the same direction. In the test, the laser, was aligned perpendicular to the surface of the materials either along X or Z axis, as shown in Fig. S1-Supplementary Material. The Raman G bands were recorded as a function of rotation angle (Φ_X, Φ_Z) and the rotation angles were used to estimate the orientation distribution function (ODF) [14, 19]. Regarding the X-axis tests, the orientation factor may vary throughout different regions, since the samples were injection moulded [20]. Hence, the tests were carried out on a number of regions across the cryo-fractured cross-sections of the samples (red dash lines in Fig. S1) to give the variation of the orientation parameter values.

3. Results

3.1 Characterisation of the filler and matrix

The three types of GNPs were examined by scanning electron microscopy as shown in Figs. S2(a-c). It can be seen that the flake size increases from M5 to M15 to M25. However, the M15 and

M25 GNPs batches seem to include a number of smaller flakes, which will decrease the average lateral size quoted by the manufacturer. Another important observation is that folded and looped structures can be found particularly in larger flake samples (Fig .S2 d and e). Overall, the three types of fillers display the stacked and agglomerated structure of many-layer graphene. The cryo-fractured cross-section of the neat elastomer can be also seen in Fig. S2(f). Two distinct morphologies can be observed, revealing the two components in the matrix and indicating that the polymer blend is not completely miscible, as expected from earlier reports [1].

The Raman spectra of the GNPs are shown in the Fig. S3(a). The G (~1580 cm^{-1}) and 2D bands (~2680 cm^{-1}) are well defined for all types of the nanoplatelets, consistent with the signature of graphitic structures. The 2D bands are broad and asymmetric suggesting that the nanoplatelets consist of many layers of graphene [11, 21, 22]. Moreover, broad and weak D bands can be observed at ~ 1360 cm^{-1} which is an indication of defects that are present in the structure. The XRD patterns of GNPs are also shown in Fig. S3(b), which display the sharp and strong peaks at $2\theta \approx 26°$ consistent with reflections from the (002) plane of graphite, while weak peaks can be seen at $2\theta \approx 42.1$, 44.3 and 54.4° corresponding to reflections from (100), (010) and (004) planes, respectively.

3.2 Characterisation of the composites

Thermogravimetric analysis was employed initially to determine the actual volume fractions of the fillers after the preparation procedure. The mass residue and volume fractions of the filler in the prepared composites are given in Table S1. It can be seen that the final mass fractions were very close to the nominal mass fractions of the nanocomposites.

The cross-sectional surfaces of cryo-fractured dumbbell samples were investigated by SEM as shown in Fig. 1. The low magnification images of the composites with highest loading (20 wt%) Figs. 1 (a-c) indicate that a uniform distribution of the fillers was achieved even at high filler

contents. The observation of different regions of the cross-section, reveals a distinct alignment of the fillers, which was induced by the shear rate distribution during the injection moulding procedure, known as a fountain flow mechanism [20, 23]. The orientation of nanoplatelets due to the fountain flow mechanism in the case of our samples can be seen in Fig S4. There are regions within the samples with different degrees of orientation of the fillers, due to the variation of shear rate generated by the combination of the injection pressure and the slightly lower temperature of the mould walls [20, 23].

The high magnification SEM images (Figs. 1 c-f) demonstrate the morphologies of the individual flakes within the matrix. Generally, the interface between the matrix and the nanoplatelets is intact, without voids or gaps, which is expected to contribute to higher reinforcement efficiency. Interestingly, the shorter flakes tend to maintain their shape after processing, as shown in Fig.1 (d), while on the other hand, the larger ones can be seen bent or form looped-folded morphologies as shown in Figs.5 (e, f). It can be also seen that the flakes tend to restack and form agglomerates, particularly at higher loadings, which will reduce the reinforcing efficiency.

(Figure 1)

3.3 Polarised Raman spectroscopy

Since it is obvious from SEM that the flakes have a preferred alignment, it is possible to quantify the orientation factor using polarised Raman spectroscopy [14]. Different regions across the cryo-fractured cross-sections of the samples were studied by using a rotation stage. Because the sample was ~5 mm in width and ~1.5 mm in thickness, the tests were carried out stepwise, every 0.25 mm from the edge to the centre of the cross-sections in the perpendicular direction of the dumbbell surfaces and the test track lines are equidistant and parallel to the two parallel sides of the rectangular cross-sections (red dash lines in both Figs. S1 and S5).

From the results shown in Fig. 2(a), it can be seen that when the laser is polarised parallel to the Z axis, there is no change in G band intensity with the rotation of Φ_Z, indicating no preferred orientation. In contrast, the G band intensity decreases from 0° to 90° and subsequently increases from 90° to 180° when the sample is rotated around the *X* axis (shown in Fig. 2b for the M5 GNP sample), which is an indication that the flakes tend to be oriented along the *X* axis. The calculated average orientation factor can be used to evaluate the effect of orientation on the reinforcing efficiency of the filler [14, 19]. The $\langle P_2(\cos\theta)\rangle$ and $\langle P_4(\cos\theta)\rangle$ values described in detail in Refs. [14, 19] are obtained by the *X* axis tests along with the curve fitting using equation (1).

$$I_{sample}(\Phi)=I_o\left\{\frac{8}{15}+\langle P_2(\cos\theta)\rangle\left(-\frac{16}{21}+\frac{8}{7}\cos^2\Phi\right)+\langle P_4(\cos\theta)\rangle\left(\frac{8}{35}-\frac{8}{7}\cos^2\Phi+\cos^4\Phi\right)\right\} \quad (1)$$

where I_o is the amplitude and assuming the surface normals are uniformly distributed around the *Z*-axis.

(Figure 2)

Subsequently, the orientation factor, η_o, is given by:

$$\eta_o=\frac{8}{15}+\frac{8}{21}\langle P_2(\cos\theta)\rangle+\frac{3}{35}\langle P_4(\cos\theta)\rangle \quad (2)$$

The orientation factors for all samples were then calculated using equation (2), and the results are listed in Tables S2-S4 and plotted in Figs. 3 (a-c). It is apparent that when moving from the edge to the centre of the cross-section, $\langle P_2(\cos\theta)\rangle$ increases and then decreases, which points out the actual variation of the orientation degrees in different regions. The results were consistent for all types of GNPs in this experiment. This trend is also in accordance with the SEM results, presented in Figs. 1 (a-c) and the shear rate profile reported in early studies on injection moulded polymer samples [20, 23]. In this experiment, the calculated average orientation factors are 0.76, 0.69 and 0.62 for M5, M15, and M25, respectively. The orientation factor values clearly imply that the degree of orientation decreases with increasing flake size, due to looped and folded morphologies

of the larger diameter flakes, which is in agreement with the results reported by Li *et al.* on GNP-reinforced natural rubbers [13].

(Figure 3)

3.4 Mechanical testing

Tensile testing was used to evaluate the mechanical properties of the materials. The stress-strain behaviour of all injection moulded samples is presented in Fig. 4(a). It can be seen that the addition of GNPs up to ~10 vol% increases the stiffness and tensile strength of the thermoplastic elastomer significantly. Overall, larger flakes are more efficient in increasing the modulus, whereas the smaller flakes contribute to better tensile strength enhancements. It is also apparent that the addition of GNPs results in a reduction of strain at failure.

The initial Young's modulus values are plotted against the volume fractions of the fillers in Fig.4 (b). As expected, in all cases, the modulus increases significantly with increasing GNP content. The modulus values of the composites are up to ~6 times higher (at 20 wt% filler loading) compared with the matrix, indicating the stiffening effect of the fillers. The reinforcement mechanism of graphene in composites is attributed to the interfacial stress transfer from the matrix to the flakes; larger platelets resulting in larger aspect ratio are beneficial for stress transfer on the basis of the well-established shear-lag theory [11, 24].

Tensile strength and strain at failure values are also plotted against GNP volume fractions in Figs. 4 (c-d). The tensile strength increases with increasing GNP loading, indicating a strong interaction between the fillers and the matrix. It has been reported that the wrinkled structure of graphene flakes can improve the tensile strength by acting as a crack propagation barrier and improve the mechanical interlocking between the matrix and the filler [25]. It can be clearly seen that the tensile strength enhancement is dependent significantly upon the flake size, particularly at high filler loadings. Tensile strength is known to depend heavily on the dispersion characteristics [15]; therefore these results indicate higher degree of aggregation of larger flakes at higher loadings and

looped/folded flake morphologies similar to the ones seen in Fig. 1(e,f). The strain at failure declines significantly with increasing filler fraction. Similar results have been observed not only for elastomeric nanocomposites but almost all polymer nanocomposites where agglomerated fillers act as failure points during elongation [9].

(Figure 4)

3.5 Raman 2D band shifts

Raman spectroscopy has been proven to be a very effective technique in assessing the stress transfer efficiency from the matrix to any type of carbon-based reinforcement [11-13, 15, 17, 26-34]. The samples the highest amount of filler (20 wt%) were strained *in situ* under a Raman spectrometer and the characteristic shifts of the Raman bands were recorded with increasing strain. A representative example of the shift of the 2D band for the composite filled with M15 flakes, can be seen in Fig. S6. The slope of the band shifts versus strain represents the stress transfer efficiency between the matrix and the filler. For each composite reinforced by M5, M15 and M25 nanoplatelets, 5 samples were tested, in order to give the average values shown in Fig. 5. It was shown that the flakes display very low 2D band shifts, with obvious scattering on the linear curve fitting, indicating the significantly lower stress transfer efficiency of this elastomeric material than the stiffer matrices of previous studies [12, 14, 28] but higher than softer matrices such as natural rubber [13]. The small values of the slope indicate the low effective modulus of GNPs within the TPE matrix, compared with pristine graphene (-60 cm^{-1}/% strain for the 2D band that corresponds to a modulus of 1050 GPa) [10, 11]. This is because the interfacial stress transfer efficiency in graphene nanocomposites depends upon the stiffness of the matrix (the effective modulus of graphene increases with increasing stiffness of the matrix), as discussed in our previous study [17].

(Figure 5)

4. Discussion

4.1 Micromechanics of reinforcement

The effect of the addition of GNPs upon the stiffness of the elastomer can be evaluated by an equation we recently developed, which is the result of the simultaneous use of the rule-of-mixtures along with the well-accepted shear-lag theory [17]. The modulus of the composite is given by:

$$E_c \approx E_m(1-V_f+\frac{s^2}{12}\frac{\eta_o}{(1+\nu)}V_f^2) \quad (3)$$

where V_f is the volume fraction of the filler, E_m and E_f are the Young's Modulus of the matrix and the filler, respectively; s is the aspect ratio of the filler in the composites; η_o is the orientation factor of the GNPs and ν is the Poisson's ratio of the matrix. Equation (3) reveals that for soft materials the composite modulus is only dependent on V_f and s^2 and independent of the filler modulus (E_m>500 MPa) [17]. This fact allows us to focus on the effective aspect ratio s_{eff} of the reinforcement, since the formation of agglomerates and the bending/folding of the flakes during processing affects the nanoplatelets critically. The results of the fitting of the experimental data with the above equation can be seen in Figs. 6 (a-c), where s_{eff} was the floating parameter. Equation 3 possesses similarities with the equation suggested by the Guth-Gold-Smallwood (GGS) theory [35, 36], in which the modulus of the composites is given by:

$$E_c=E_m(1+0.67fV_f+1.42f^2V_f^2) \quad (4)$$

where f is length/breadth of the platelet-like or rod-like filler, which can be considered analogous to the aspect ratio of the filler. The fitting of the experimental data with the GGS theory can be seen in Fig.6 (d) for the 2265-M5 samples, while the rest of the results can be found in Fig. S7.

Both equations fit the experimental results quite well and the effective aspect ratio of the fillers increases systematically from M5 to M15 to M25, attributing better enhancement to the stiffness of the composites. However, the values are significantly lower than the ones expected, which should be in the order of 10^3, based on the dimensions of the nanoplatelets measured in our

previous study [17]. The reason for the relatively small values of aspect ratio can be attributed to the restacking and agglomeration of the flakes that is unavoidable, especially at higher filler loading and to the additional presence of looped and folded flakes in the composites, that can pre-exist in the batches of the nanoplatelets or can also originate from the shear forces applied to the flakes during melt mixing/injection moulding. As shown in Fig. 5(f), the looped/folded flakes can even form hollow structures, resulting in significant reductions of the aspect ratio values.

(Figure 6)

The fitted values of the effective aspect ratio for both equations can be used to evaluate the reinforcing efficiency of the GNPs. Nevertheless, the Guth-Gold-Smallwood theory is based on the effect of pairs of spherical fillers [35, 36], which is an analogy of rod-like fillers, rather than relatively thin nanoplatelets. This is why the fitted aspect ratio *f*, obtained from the GGS equation is significantly lower than that of the GNP flakes. Moreover, from Fig.6 it can be seen that the normalized modulus of the nanocomposites filled with 5 wt% and 10 wt% lie above the expected theoretical values. This observation indicates a more homogeneous dispersion of the filler at lower GNP loadings [12, 15, 37]. The phenomenon can be also inspected from Fig. 7, where the experimental data have been fitted for every specimen individually. In order to obtain the effective aspect ratio at each filler content, we noted that s_{eff} decreases with increasing filler fractions, which reduces the reinforcing efficiency. The respective effective aspect ratios can be seen on Fig. 7 for each sample. The reduction of s_{eff} with increasing loading was expected, as larger loadings can lead to pronounced agglomeration, restacking and folding of the flakes, which obviously reduce their ultimate aspect ratio.

(Figure 7)

4.2 Stress-induced 2D Raman band shifts

In our previous work, we showed that on the basis of the shear-lag theory, for soft matrices reinforced by graphene nanoplatelets, the Young's modulus of the flakes obtained from Raman experiments (E_R) is higher than the filler modulus (E_f) acquired from tensile testing [17]. The Raman modulus of the graphene flakes is given by:

$$E_R = -\frac{d\omega_{2D}}{d\varepsilon}\frac{1050}{-60}\,\text{GPa} \quad (5)$$

where $-d\omega_{2D}/d\varepsilon$ is the 2D Raman band shift rate per % composite strain for any type of graphene. The filler modulus from tensile tests, according to the simple rule of mixtures can be calculated by

$$E_f = \frac{E_c - E_m(1-V_f)}{V_f} \quad (6)$$

where V_f is the volume fraction of the filler, E_m and E_c are the Young's modulus of the matrix and the filler, respectively. The theoretical E_R and E_f derived by shear lag theory are given by [17],

$$E_f \approx \eta_o \frac{s^2}{12}\frac{1}{1+\nu}\frac{t}{T}E_m \quad (7)$$

and

$$E_R \approx \eta_o \frac{s^2}{8}\frac{1}{1+\nu}\frac{t}{T}E_m \quad (8)$$

where t is the thickness of the flake and T is the thickness of the polymer layer surrounding the flake in the model nanocomposite. Equations (7) and (8) predict that the Raman modulus is higher than the filler modulus obtained from tensile testing. If we take the E_R/E_f ratio from the two equations, then $E_R \approx 1.5E_f$. The experimental data of E_R and E_f from the samples with the highest filler contents are all listed in Table 1. The experimentally obtained values of E_R and E_f reveal that the effective modulus of graphene within this quite soft TPE matrix ($E_m \approx 10$ MPa) is in the order of hundreds of MPa, which is three to four orders of magnitude lower than the intrinsic modulus of monolayer graphene (1050 GPa) [10, 11]. The reason for the low E_f and E_R values is that the shear modulus of the elastomeric matrix is very low; therefore, the shear stress transferred from the

matrix to the flakes through the TPE/GNP interface, according to the shear lag theory, is relatively low [13, 17]. Based on this, even though the absolute enhancement of the mechanical properties of soft materials in terms of percentage is almost always impressive, the superlative mechanical properties of graphene and graphene nanoplatelets are not realised in these systems.

It should also be stated that the Raman band shift experiments were carried out probing flakes axially aligned on the sample surface. This means that the flakes that were tested should be considered nearly perfectly orientated ($\eta_o \approx 1$), whereas the calculated filler modulus E_f values have actually taken the orientation factors of the bulk composites into account. Therefore, the actual relationship between experimental E_R and E_f should be given by

$$E_R \approx 1.5 E_f / \eta_o \quad (9)$$

where η_o is the overall orientation factor of the bulk composites.

(Table 1)

The results from the use of the $E_R \approx 1.5 E_f / \eta_o$ relationship show good consistency with the measured E_R values (Table 1) especially for smaller flakes and the differences between the data can originate either from disoriented flakes that have been tested or due to the rough and wrinkled surface of the nanoplatelets [38]. Another factor of discrepancy can be the length effects that are known to reduce the efficiency of reinforcement from the nanoplatelets. The agreement between the theoretical and experimental values is another indication that the orientation factor calculated from the polarized Raman experiments are very close to reality, for the bulk composites.

5. Conclusions

A series of GNP-reinforced thermoplastic elastomers have been successfully prepared by melt mixing. The SEM images suggest that the dispersion of the GNPs is quite homogeneous, while the alignment of the fillers is induced by shear during the injection moulding procedure. The interface

between the nanoplatelets and the matrix is most of the times intact, while looped and folded morphologies can be found for larger flakes, which are expected to reduce their intrinsic properties. Polarised Raman spectroscopy has been employed to quantify the orientation factor of the injection moulded samples and we showed that the orientation profile throughout the cross-section was consistent with the trend of the shear rate profile from injection moulding. Larger flakes have lower degree of orientation, again as a result of looped or folded structures.

The mechanical properties from tensile tests revealed that the introduction of GNPs into the TPE gave rise to significant improvements in its stiffness (6 times higher, up to 10 vol% loading) and strength compared to the matrix. Overall, the larger flakes contribute to better enhancements in the stiffness while smaller flakes lead to a better increase of strength. The modulus values were studied with an equation derived by analytical methods and described in detail in our previous work, by combining the shear lag theory with the well-accepted rule-of-mixtures [17]. It was revealed that the composite modulus has a quadratic relationship with the volume fraction of the filler and depends heavily on the aspect ratio of the filler, which is similar as the classical Guth-Gold theory. The effective aspect ratio is found to be of the order of 100. With increasing loading, the average effective aspect ratio of the GNPs is reasonably reduced as a result of restacking, agglomeration and folding of the GNPs, which can explain the effect of reduced reinforcing efficiency on both stiffness and strength. Finally, both the filler modulus from the tensile testing and Raman modulus of the bulk composites measured by 2D band shifts were found to be lower compared to composites based on stiff polymers but higher than those based on very soft matrices (ie. silicon rubber) due to different shear modulus of the materials. The experimental data have also been analysed and show a good consistency with theory.

It can be concluded that the reinforcement efficiency of the GNPs on a thermoplastic elastomer matrix is highly dependent on the filler geometry and also the processing method. The improvements of the stiffness and strength, to a large extent, rely on the effective aspect ratio of

the flakes. The processing method, on the other hand, affects the dispersion, orientation and further intercalation of the filler significantly, which is of a great significance in determining the filler geometry in the bulk nanocomposites. The composites produced show great promise in terms of their mechanical properties and can be considered as high-performance engineering plastics that can be attractive to a number of high-tech industries such as automobile or aerospace, as well as their possible use in conventional consumer goods.

Acknowledgements

This research has been supported by funding from the European Union Horizon 2020 Programme under the Graphene Flagship grant agreement n°604391 and the EPSRC (award no. EP/I023879/1). One of the authors (M. Liu) is grateful to the China Scholarship Council for financial support. All research data supporting this publication are available within this publication.

References

[1] Akkapeddi M. Commercial polymer blends. Polymer blends handbook: Springer; 2003. p. 1023-115.

[2] Drobny JG. Handbook of thermoplastic elastomers: Elsevier; 2014.

[3] Koerner H, Price G, Pearce NA, Alexander M, Vaia RA. Remotely actuated polymer nanocomposites—stress-recovery of carbon-nanotube-filled thermoplastic elastomers. Nat Mater 2004;3(2):115-20.

[4] Frogley MD, Ravich D, Wagner HD. Mechanical properties of carbon nanoparticle-reinforced elastomers. Compos Sci Technol 2003;63(11):1647-54.

[5] Costa P, Silva J, Sencadas V, Simoes R, Viana J, Lanceros-Méndez S. Mechanical, electrical and electro-mechanical properties of thermoplastic elastomer styrene–butadiene–styrene/multiwall carbon nanotubes composites. J Mater Sci 2013;48(3):1172-9.

[6] Khan U, May P, O'Neill A, Coleman JN. Development of stiff, strong, yet tough composites by the addition of solvent exfoliated graphene to polyurethane. Carbon 2010;48(14):4035-41.

[7] Katbab A, Nazockdast H, Bazgir S. Carbon black-reinforced dynamically cured EPDM/PP thermoplastic elastomers. I. Morphology, rheology, and dynamic mechanical properties. J Appl Phys 2000;75(9):1127-37.

[8] Novoselov KS, Geim AK, Morozov SV, Jiang D, Zhang Y, Dubonos SV, et al. Electric field effect in atomically thin carbon films. Science 2004;306(5696):666-9.

[9] Papageorgiou DG, Kinloch IA, Young RJ. Graphene/elastomer nanocomposites. Carbon 2015;95:460-84.

[10] Lee C, Wei X, Kysar JW, Hone J. Measurement of the elastic properties and intrinsic strength of monolayer graphene. Science 2008;321(5887):385-8.

[11] Gong L, Kinloch IA, Young RJ, Riaz I, Jalil R, Novoselov KS. Interfacial stress transfer in a graphene monolayer nanocomposite. Adv Mater 2010;22(24):2694-7.

[12] Ahmad SR, Xue C, Young RJ. The mechanisms of reinforcement of polypropylene by graphene nanoplatelets. Mater Sci Eng, B 2017;216:2-9.

[13] Li S, Li Z, Burnett TL, Slater TJ, Hashimoto T, Young RJ. Nanocomposites of graphene nanoplatelets in natural rubber: microstructure and mechanisms of reinforcement. J Mater Sci 2017;52(16):9558-72.

[14] Li Z, Young RJ, Wilson NR, Kinloch IA, Vallés C, Li Z. Effect of the orientation of graphene-based nanoplatelets upon the Young's modulus of nanocomposites. Compos Sci Technol 2016;123:125-33.

[15] Papageorgiou DG, Kinloch IA, Young RJ. Mechanical properties of graphene and graphene-based nanocomposites. Prog Mater Sci 2017;90:75-127.

[16] Young RJ, Kinloch IA, Gong L, Novoselov KS. The mechanics of graphene nanocomposites: a review. Compos Sci Technol 2012;72(12):1459-76.

[17] Young RJ, Liu M, Kinloch IA, Li S, Zhao X, Vallés C, et al. The mechanics of reinforcement of polymers by graphene nanoplatelets. Compos Sci Technol 2018;154:110-6.

[18] Lacayo-Pineda J. Filler Dispersion and Filler Networks. Encyclopedia of Polymeric Nanomaterials 2015:771-6.

[19] Li Z, Young RJ, Kinloch IA, Wilson NR, Marsden AJ, Raju APA. Quantitative determination of the spatial orientation of graphene by polarized Raman spectroscopy. Carbon 2015;88:215-24.

[20] Kenig S. Fiber orientation development in molding of polymer composites. Polym Compos 1986;7(1):50-5.

[21] Ferrari AC, Meyer J, Scardaci V, Casiraghi C, Lazzeri M, Mauri F, et al. Raman spectrum of graphene and graphene layers. Phys Rev Lett 2006;97(18):187401.

[22] Malard L, Pimenta M, Dresselhaus G, Dresselhaus M. Raman spectroscopy in graphene. Phys Rep 2009;473(5):51-87.

[23] Tadmor Z. Molecular orientation in injection molding. J Appl Polym Sci 1974;18(6):1753-72.

[24] Cox H. The elasticity and strength of paper and other fibrous materials. Br J Appl Phys 1952;3(3):72.

[25] Wakabayashi K, Pierre C, Dikin DA, Ruoff RS, Ramanathan T, Brinson LC, et al. Polymer−Graphite Nanocomposites: Effective Dispersion and Major Property Enhancement via Solid-State Shear Pulverization. Macromolecules 2008;41(6):1905-8.

[26] Deng L, Eichhorn SJ, Kao C-C, Young RJ. The effective Young's modulus of carbon nanotubes in composites. ACS Appl Mater Interfaces 2011;3(2):433-40.

[27] Young RJ. Deformation Mechanisms of Carbon Fibres and Carbon Fibre Composites. The Structural Integrity of Carbon Fiber Composites: Springer; 2017. p. 341-57.

[28] Papageorgiou DG, Kinloch IA, Young RJ. Hybrid multifunctional graphene/glass-fibre polypropylene composites. Compos Sci Technol 2016;137:44-51.

[29] Young RJ, Deng L. Carbon Nanotubes and Nanotube-Based Composites: Deformation Micromechanics. Structure and Multiscale Mechanics of Carbon Nanomaterials: Springer; 2016. p. 51-74.

[30] Young RJ. Carbon Fibre Composites: Deformation Micromechanics Analysed using Raman Spectroscopy. Structure and Multiscale Mechanics of Carbon Nanomaterials: Springer; 2016. p. 29-50.

[31] Young RJ, Deng L, Wafy TZ, Kinloch IA. Interfacial and internal stress transfer in carbon nanotube based nanocomposites. J Mater Sci 2016;51(1):344-52.

[32] Tanaka F, Okabe T, Okuda H, Ise M, Kinloch IA, Mori T, et al. The effect of nanostructure upon the deformation micromechanics of carbon fibres. Carbon 2013;52:372-8.

[33] Vallés C, Kinloch IA, Young RJ, Wilson NR, Rourke JP. Graphene oxide and base-washed graphene oxide as reinforcements in PMMA nanocomposites. Compos Sci Technol 2013;88:158-64.

[34] Vilatela J, Deng L, Kinloch I, Young R, Windle A. Structure of and stress transfer in fibres spun from carbon nanotubes produced by chemical vapour deposition. Carbon 2011;49(13):4149-58.

[35] Smallwood HM. Limiting law of the reinforcement of rubber. J Appl Phys 1944;15(11):758-66.

[36] Guth E. Theory of filler reinforcement. J Appl Phys 1945;16(1):20-5.

[37] Papageorgiou DG, Terzopoulou Z, Fina A, Cuttica F, Papageorgiou GZ, Bikiaris DN, et al. Enhanced thermal and fire retardancy properties of polypropylene reinforced with a hybrid graphene/glass-fibre filler. Compos Sci Technol 2018;156(1):95-102.

[38] Li Z, Kinloch IA, Young RJ, Novoselov KS, Anagnostopoulos G, Parthenios J, et al. Deformation of wrinkled graphene. ACS Nano 2015;9(4):3917-25.

Figure Legends

Figure 1. SEM images of cryo-fractured cross-section of the injection moulded composites: (a-c) low magnification images of the composites (2265-M5-GNP20) showing preferred orientation of the flakes in accordance with fountain flow mechanism; (e-f) High magnification images of M5, M15 and M25 GNPs in the composites showing the interface between the filler and the matrix and preferred morphologies dependent on the sizes of the fillers.

Figure 2. Representative fitting of normalized G band intensities parallel to the (a) Z and (b) X axis as a function of rotational angle for M5 GNPs.

Figure 3. Orientation degrees of (a-c) M5, M15 and M25 samples showing variation of the orientation factor against the position of the test spots.

Figure 4. (a) Stress-strain curves of the materials; (b-d) Plots of the values of stiffness, tensile strength and strain at failure against volume fractions of the GNPs.

Figure 5. 2D Raman band shifts of (a-c) M5, M15 and M25 flakes respectively against the composite strain. Different colours represent different sets of measurements. The fittings were carried out based on all measurements for each type of GNP.

Figure 6. Normalized Young's Modulus against the volume fraction of the filler and fitted data using equation (3) for (a) 2265-M5, (b) 2265-M15 and (c) 2265-M25 samples; and fitted using equation (4) for (d) 2265-M5.

Figure 7. Individually fitted data with different values of aspect ratio for different filler loadings of (a-c) M5, M15 and M25 reinforced elastomer composites using equation (3).

List of Tables

Table 1. Raman 2D band shift values and the corresponding calculated Raman modulus along with the filler modulus acquired from the tensile testing.E_R and E_f at 20 wt% GNP loading are calculated using equation (5) and (6), respectively. $1.5E_f/\eta_o$ is the theoretically calculated E_R (assuming the flake is perfectly aligned) based on equation (7), (8) and (9).

	M5	M15	M25
Band shift (cm^{-1}/% strain)	-0.036 ± 0.003	-0.040 ± 0.005	-0.050 ± 0.006
E_R (MPa)	630 ± 53	700 ± 88	875 ± 105
E_f (MPa)	336 ± 37	383 ± 40	457 ± 111
Theoretical E_R ($1.5E_f/\eta_o$ (MPa))	663 ± 74	833 ± 87	1106 ± 269

Figure 1

Click here to download high resolution image

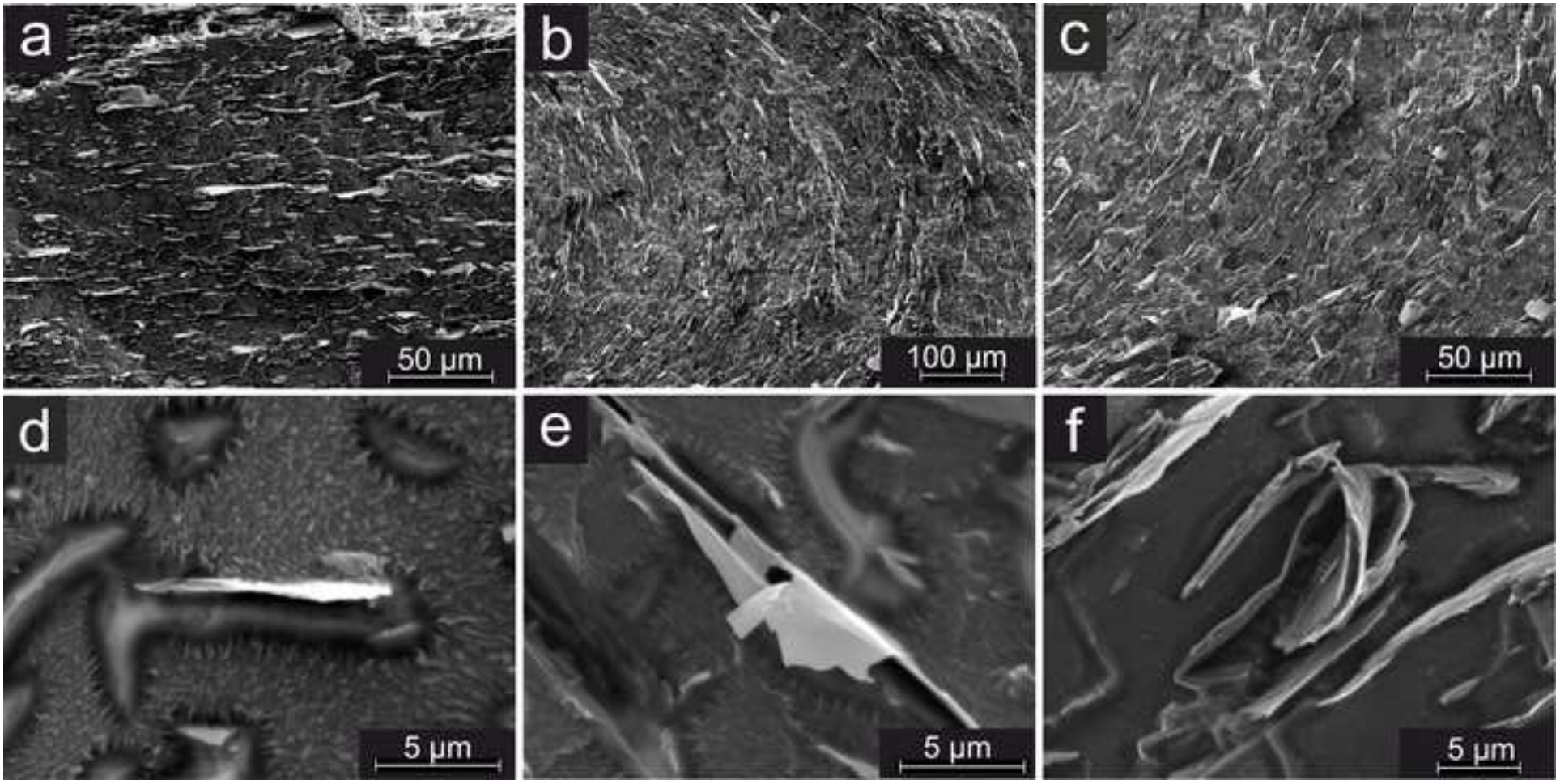

Figure 2

Click here to download high resolution image

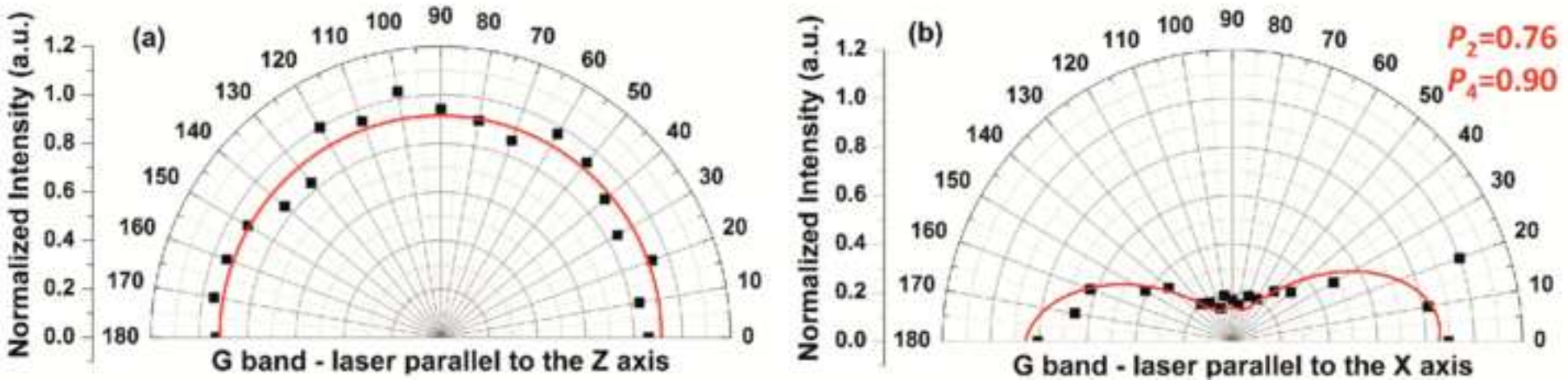

Figure 3

Click here to download high resolution image

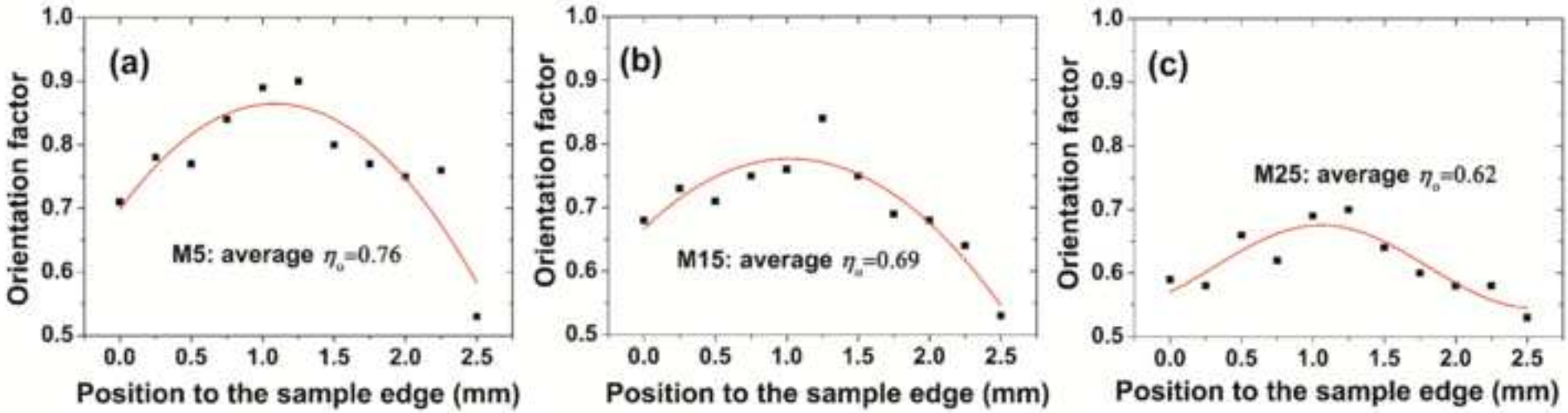

Figure 4

Click here to download high resolution image

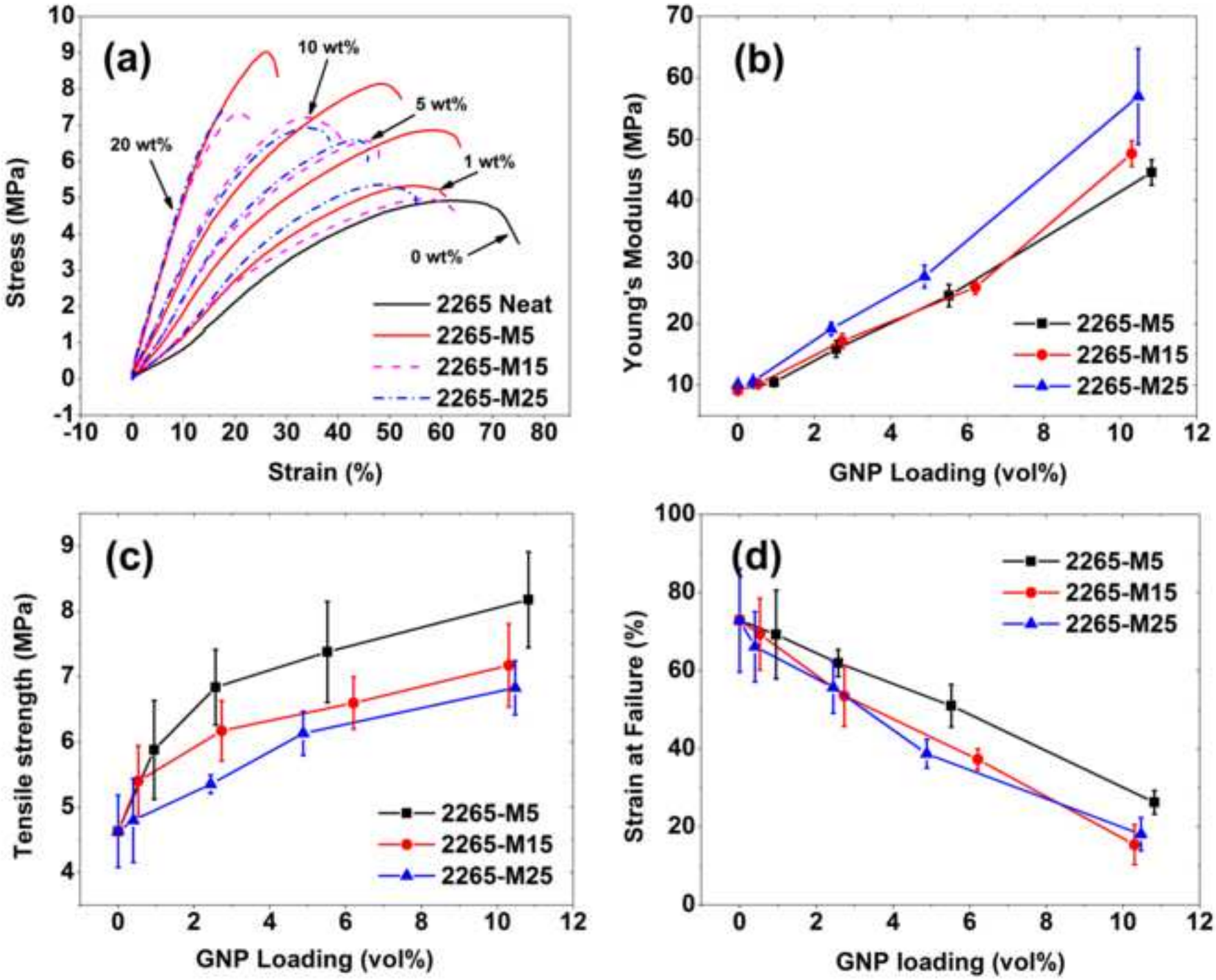

Figure 5

Click here to download high resolution image

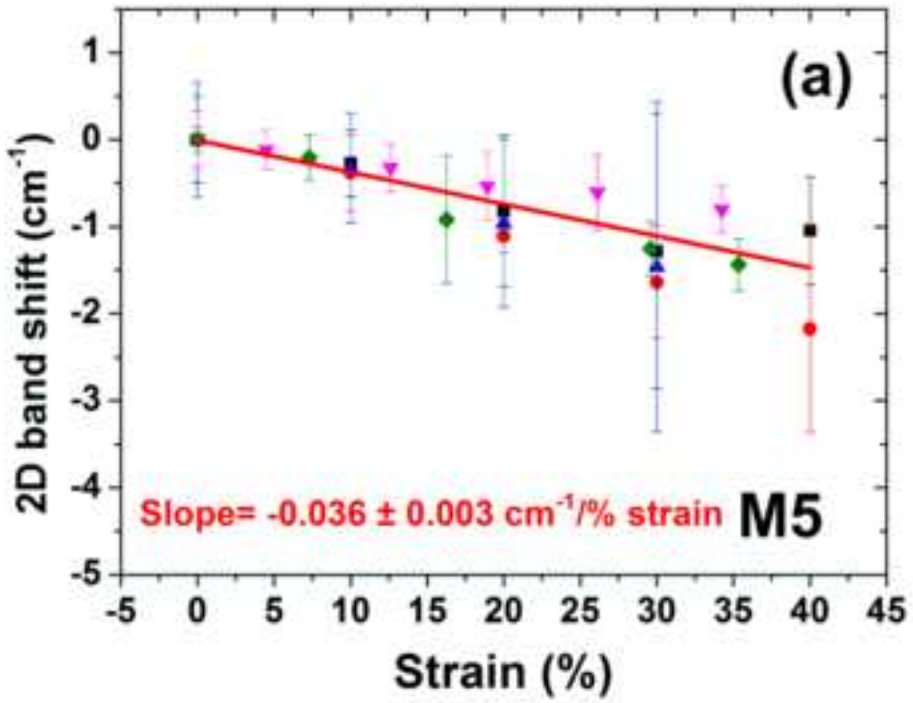

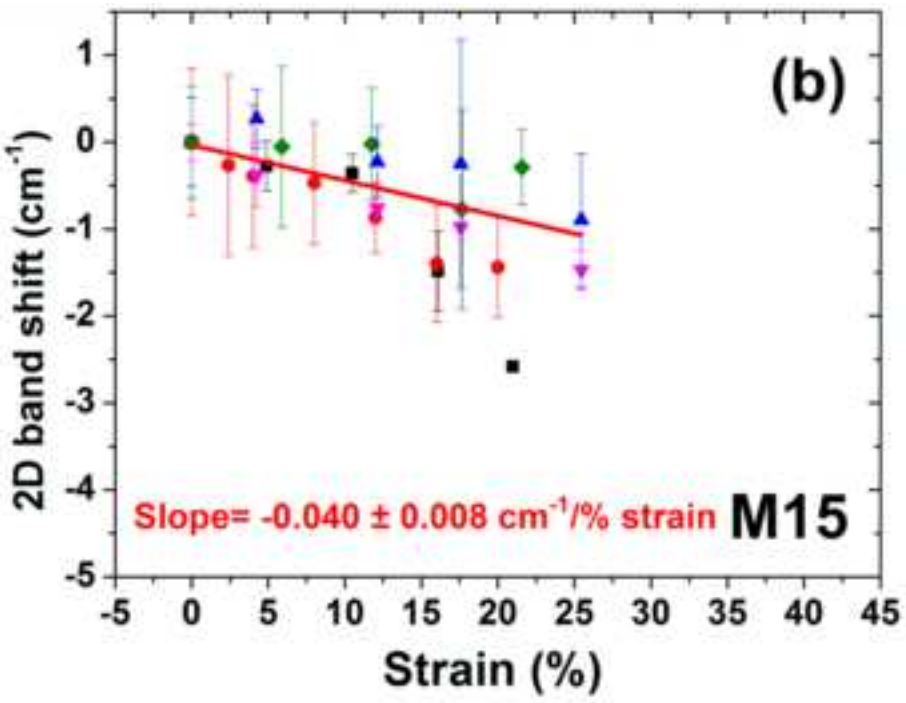

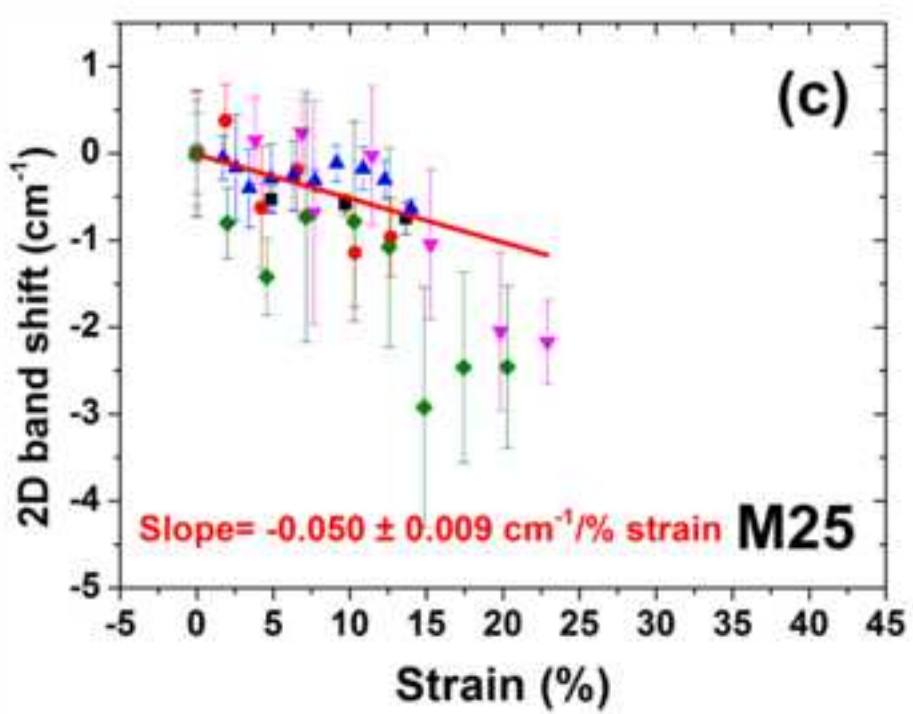

Figure 6

Click here to download high resolution image

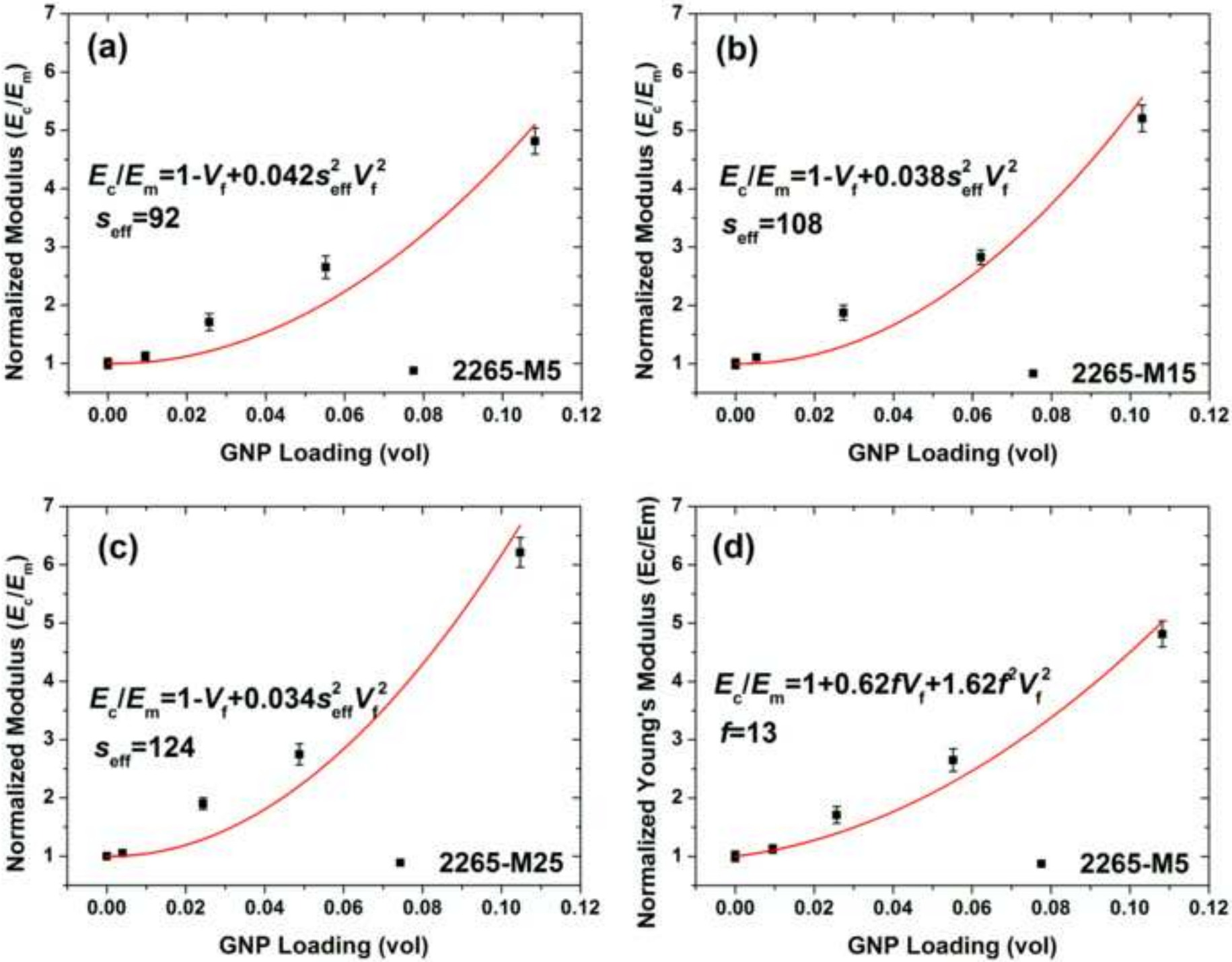

Figure 7

Click here to download high resolution image

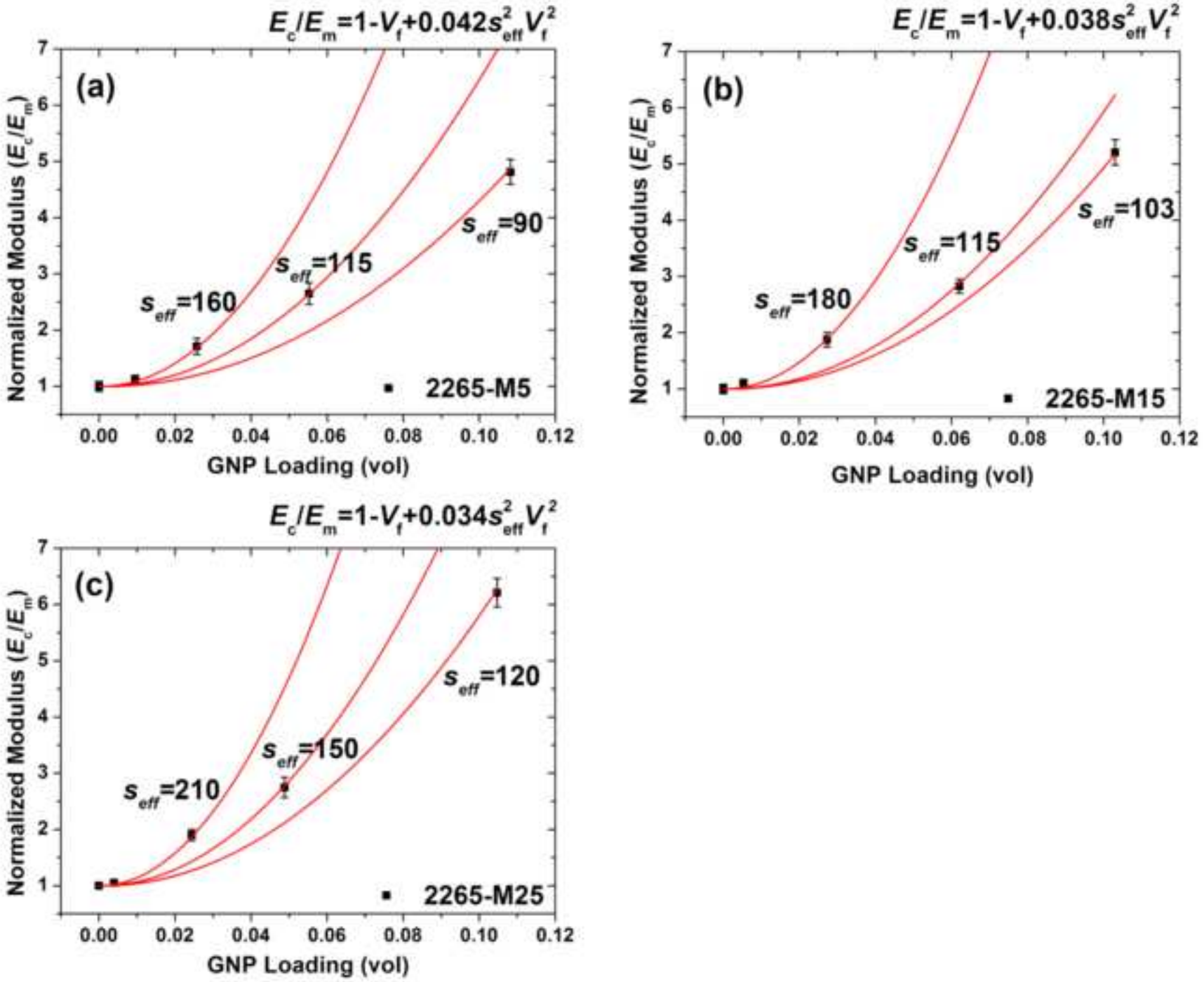

Supplementary Information

Click here to download Data in Brief: TPE-GNP Supporting Information DGP5.docx